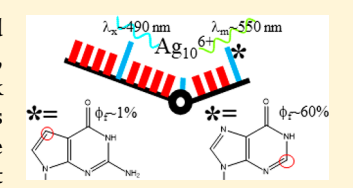
A DNA-Encapsulated Silver Cluster and the Roles of Its Nucleobase Ligands

Jeffrey T. Petty,*,†,|| Mainak Ganguly,†,|| Ahmed I. Yunus,† Chen He,† Peter M. Goodwin,‡ Yi-Han Lu,[§] and Robert M. Dickson[§]

Supporting Information

ABSTRACT: Silver clusters consisting of ~10 atoms are readily bound by and encapsulated within DNA strands to yield strong absorption and emission. The coordination environments, however, are poorly understood, so cluster adducts can only be empirically tuned. This work describes the C₄AC₄TC₃G strand that templates a particular cluster adduct. Its sequence has three types of nucleobases with distinct roles—tracts of cytosines that collectively coordinate the cluster, thymine acting as a junction in the overall strand, and the adenine/guanine pair that exclusively forms the cluster. In relation to the native oligonucleotide, the DNA-silver cluster



complex diffuses faster and is more compact, thus suggesting that the strands fold because of the cluster. The Ag₁₀⁶⁺ adduct emits with $\lambda_{\rm ex}/\lambda_{\rm em} = 490/540$ nm, a 19% quantum yield, and a biexponential 1.1/2.1 ns lifetime. The electronic environment for the cluster is controlled by the heteroatoms in the adenine and guanine. Most significantly, the N7 and the N2 in the guanine change the fluorescence quantum yield by 60-fold and shift the fluorescence lifetime by ~3.8 ns. Thus, our studies discern distinct spectroscopic and structural roles for the nucleobase ligands in C₄AC₄TC₃G, and these findings may help develop new DNA templates for other silver cluster adducts.

INTRODUCTION

Noble metals are prized for their luster, which arises because the valence electrons efficiently reradiate visible light when they move between the electronic bands. However, when bulk metals are shrunk to nm and smaller dimensions, molecular spectra emerge. $^{1-4}$ For example, silver clusters with ~ 10 atoms fluoresce because their valence electrons transition between discrete HOMO-LUMO states, as with organic dyes. 5-11 These spectra span the visible and near-infrared spectral regions because of the distinctive electronic states within silver molecules. A diverse suite of noble metal chromophores can be realized by controlling cluster size and shape, as species differing by only a single atom or those having nearly isoenergetic isomers exhibit distinct and wide-ranging spectra. 12 Our studies focus on ligands that can trap and protect specific clusters and arrest their agglomeration. 12-15 Because of the strength of the covalent bond, thiols have been particularly effective in noble metal nanoparticle creation but often at the cost of bright fluorescence, as charge transfer interactions often lead to low quantum yields, large Stokes shifts, and long luminescence lifetimes. 16-21

Biopolymers are polydentate ligands that not only stabilize but also template distinct types of noble metal clusters. These scaffolds likely harbor distinctive coordination environments because of their covalently linked backbones and thereby create new species inaccessible via small molecule ligands. We study monodisperse oligonucleotides that bind and locally concentrate Ag+, which then coalesce following chemical reduction.²² The DNA protects the metallic cores in aqueous, buffered, and biological solutions.²³⁻²⁵ Beyond acting as a protective shell, oligonucleotides dictate the cluster size and geometry, thereby imprinting the optical spectra and photophysics of their adducts. Three distinctive features of the DNA-Ag interaction have been discovered. 22,23,25-29 First, altering the primary DNA sequence tunes the cluster spectra across the violet to near-infrared.²⁹⁻³¹ These chromophores are bright with fluorescence quantum yields of 10-90%, fluorescence lifetimes of ~2 ns, and extinction coefficients of ~10⁵ M⁻¹ cm^{-1,32,33} Second, changes in DNA structure can alter cluster adduct brightness, as complementary strands hybridize with the DNA host and toggle the cluster adduct between dark and bright states with turn-on ratios over ~1000.^{24,34} These conjugates are readily synthesized and can be used in situ, so they are viable alternatives to expensive molecular beacons that must be prederivatized with organic dyes.³⁵ Third, the Ag–DNA interaction produces μs-lived dark electronic states that can be used to enhance fluorescence detection.³⁶ These dark states are populated via laser excitation

Received: October 2, 2018 Revised: November 6, 2018 Published: November 13, 2018

Department of Chemistry, Furman University, Greenville, South Carolina 29163, United States

[‡]Center for Integrated Nanotechnologies, Mail Stop K771, Los Alamos National Laboratory, Los Alamos, New Mexico 87545, United States

[§]School of Chemistry and Biochemistry and Institute for Bioengineering & Bioscience, Georgia Institute of Technology, Atlanta, Georgia 30332, United States

and subsequently depopulated via longer wavelength coillumination. This sequential, two-laser excitation boosts the net fluorescence and drastically increases sensitivity through modulation or time-gating that discriminates against background emission. 37,38

DNA strands coordinate silver clusters via their nucleobases that are anchored to the phosphodiester backbone, and the DNA sequence and structure define binding sites for specific silver clusters. Individual nucleobase ligands bind silvers with different affinities that depend on the basicities and protonation states of the heteroatoms. 31,39-42 Multiple nucleobases coordinate a single cluster so that the strands fold and dimerize around their adduct. Furthermore, minor sequence changes elicit large spectral changes.31,42 Herein, we describe the sequence and structure of a family of DNA scaffolds that preferentially form a silver cluster with a single absorption band at 490 nm. These clusters are part of a larger suite of chromophores that span the visible and nearinfrared spectral regions, and these DNA-protected chromophores are promising biological labels and sensors with strong fluorescence brightness that can be further enhanced via sequential two-photon excitation. 31,36-38,45-48 Additionally, they signal changes in their environment with up to 103-fold stronger emission via hybridization. 23,24 Our studies consider how the 490 nm cluster interacts with a specific class of DNA hosts. The oligonucleotides are single-stranded and thus eliminate canonical base pairing that could disrupt nucleobase-silver coordination. Our key finding is that these sequences are divided into tracts and three types of nucleobase ligands appear to control the organization and photophysics of this hybrid DNA-cluster chromophore.

■ EXPERIMENTAL SECTION

Synthesis. Desalted oligonucleotides were purchased from Integrated DNA Technologies. These samples were dissolved in deionized water, and DNA concentrations were determined from the molar absorptivities on the basis of the nearestneighbor approximation. 49 Most oligonucleotides were singlestranded, but one was a mixed single-/double-stranded construct. The strand CCCCACCCT CCCGTTCGGG folds at the TT junction to form a CCCG-GCCC duplex with a CCCCACCCCT overhang (see Figure S1 for structure). DNA-silver cluster conjugates were synthesized by combining the oligonucleotide and AgNO3 at a 1:8 relative ratio, with a DNA concentration of 30 μ M in either water or a 1 mM cacodylate buffer at pH 7. An aqueous solution of NaBH₄ is added to give a final concentration of 4 BH₄-:oligonucleotide. The solution is then placed in a highpressure reactor with 400 psi of O₂ for ~3 h.⁵⁰ Abasic sites were introduced at specific locations in the oligonucleotide by substituting the target nucleobase with a uracil. This nucleobase was then excised using uracil DNA glycosylase.⁵¹

Characterization. Absorption spectra were acquired on a Cary 50 from Varian, and emission spectra were acquired on a FluoroMax-3 from Jobin-Yvon Horiba. Size exclusion chromatography used a 300 mm, 7.8 mm inner diameter column (BioSep, Phenomenex) on a high performance liquid chromatography system (Prominence, Shimadzu) using a 10 mM cacodylate buffer at pH 7 with 40 mM NaClO $_4$ to minimize matrix adsorption. Absorbance measurements of the separated species were made using the SPD-M20A detector. For the thymine oligonucleotides dT_{10} , dT_{15} , dT_{20} , and dT_{30} , the averages and standard deviations of the retention times

correlated linearly with the hydrodynamic radii, allowing their use as a size standard to determine the radii of the cluster conjugates. Mass spectra were collected using Q-TOF G2-S (Waters) and analyzed with MassLynx V4.1. $^{43,49,52-54}$

Time-correlated single-photon counting measured the fluorescence lifetimes and anisotropies. A pulsed 470 nm laser (PicoQuant) excited the samples at 10 MHz. The laser was vertically polarized, and the emission was collected with the emission polarizer set to the magic angle at ~55°. The fluorescence was collected at 90° relative to the excitation and was spectrally filtered using a 525 \pm 20 nm bandpass filter. The emission was detected by a photomultiplier tube (R928, Hammatsu), the output of which was inverted before being processed by a photon counting board (HydraHarp). The instrument response function (IRF) was recorded using colloidal silica (Aldrich). The fwhm of the IRF was ~150 ps. The fluorescence decay was determined through IRF reconvolution fitting of the measured decay (FluoFit). The anisotropy measurements were made using vertically and horizontally polarized excitation along with vertically and horizontally polarized emission. The G-factor accounts for the detection efficiency of vertically and horizontally polarized emission and was ~1 for our filter-based instrument. The fluorescence decays were reconvolved with the IRF and used to calculate the anisotropy (FluoFit).

Two-focus fluorescence correlation spectroscopy was used to measure the diffusion coefficients of fluorescent species freely diffusing through a pair of laterally offset excitation volumes. These submicron diameter, orthogonally polarized excitation focal spots were formed using a differential interference contrast prism (U-DICTHC, Olympus) and a ×60, 1.2 NA water immersion objective (UPLANSAPO, Olympus) to focus a pair of orthogonally polarized, repetitively pulsed (~100 ps width) 485 nm laser excitation beams (P-C-485B, Picoquant) into the liquid sample droplet deposited on a glass coverslip. The sample emission was spatially filtered using a 200 μ m diameter pinhole located in the image plane of the inverted microscope (IX-71, Olympus). Sample fluorescence was isolated from scattered 485 nm excitation light using a 30 nm wide bandpass filter centered at 550 nm. The fluorescence was split into approximately equal parts using a 50% beam splitter and focused onto a pair of single-photon-counting avalanche photodiode detectors (SPCM-AQR-14, PerkinElmer). Time-correlated single-photon-counting electronics (Pico-Harp 300, Picoquant) and software (SymPhoTime 64, Picoquant) were used to collect and record photon arrival times from the samples. The samples were excited at 485 nm using alternating polarization pulsed interleaved excitation at 40 MHz with a total average power of \sim 10 μ W. Arrival times of the detected fluorescence photons with respect to the interleaved excitation pulses were used to determine the identity of the excitation focus from which the emission originated. This information was used to calculate fluorescence intensity autocorrelations for each of the excitation spots as well as intensity cross-correlations between the two foci. The diffusion coefficient of the fluorescent species was obtained from a global fit to these correlations following the methods developed by Dertinger et al.⁵⁵ The lateral separation (390 nm) of the excitation foci in our setup was determined by a global fit of the intensity correlations obtained from a dilute aqueous solution of rhodamine-110 with a known diffusion coefficient in water (440 μ m²/s @ 22.5 °C). ⁵⁶ We corrected this value to 411 μ m²/s @ 20 °C using the temperature

dependent viscosity of water, since our measurements were made at 20 °C. The global fits to the intensity correlations were done in MATLAB using routines (FCSFIT.m) obtained from Jörg Enderlein.

RESULTS

DNA-cluster complexes were characterized by electronic spectroscopy, mass spectrometry, and chromatography. Silver clusters typically exhibit extinction coefficients of ~10⁵ M⁻¹ cm⁻¹, so absorption spectra comprehensively distinguish conjugates at $1-10 \mu M$ concentrations.⁵¹ Silver clusters can also fluoresce, and fluorescence spectra, quantum yields, and lifetimes reveal changes in their electronic environment. Clusters form within a chiral DNA template, and visible circular dichroism characterizes the nucleobase-cluster coordination. The oligonucleotides are monodisperse, so electrospray ionization mass spectrometry yields the stoichiometries of the DNA-Ag cluster adducts. Furthermore, the polyelectrolyte DNA backbone readily exchanges H+ with the solvent, so the number of phosphate-bound H+ indirectly measures the cluster charge. The DNA has ~4-fold larger mass and significantly larger physical extent than the cluster, thereby dominating the overall structure of the conjugate. Size exclusion chromatography, fluorescence correlation spectroscopy, and fluorescence anisotropy quantify how the DNA shape is molded by its cluster adduct.

Primary Sequence-Repeated Cytosine Tracts. Our goal was to synthesize a bright silver cluster fluorophore with green emission. One such species has $\lambda_{\rm ex}/\lambda_{\rm em} = 490/540$ nm, an ~ 2 ns fluorescence lifetime, and an ~20% fluorescence quantum yield, and it has been synthesized in a hybrid DNA construct with a duplex and a dangling C₄AC₄T appendage (Figures 1A and S1). 52 We sought to synthesize an analogous cluster within a purely single-stranded DNA, which would allow us to interrogate the cluster coordination environment. 23,24,52,57 We began with C₄AC₄T alone because such appendages control the cluster spectra in the hybrid duplex/single-stranded constructs.⁵⁸ However, this sequence was inadequate, possibly because it is too short to form clusters (Figure S1).⁵¹ We thus extended this strand by adding an additional C₄X motif to create $C_4AC_4TC_4X$ with X = A, T, G, and C. These strands differ by a single nucleobase yet yield distinctive chromophores (Figure 1A). Only the X = G strand produces the target chromophore with strong absorption at ~490 nm, like the hybrid duplex/single-stranded construct (Figure 1A). Starting with this favored strand, the DNA sequence was varied to optimize cluster absorption at 490 nm, and our studies were guided by the repeated C₄X organization. Specifically, the number and continuity of the cytosines and the terminating nucleobases in each tract were varied.

Numbers and Continuity of Cytosines. $C_4AC_4TC_4G$ produces the target $\lambda = 490$ nm cluster along with a competing violet-absorbing species, but this spectrum and cluster environment change with the number of cytosines (emphasized with underlining). When the third tract is shortened from CCCCG to CCCG, the resulting $C_4AC_4TC_3G$ develops a stronger 490 nm band relative to the violet absorption (Figure 1B). Further truncation is detrimental, however, as $C_4AC_4TC_2G$ eliminates the target 490 nm species in lieu of alternate species. The other tracts behave similarly. Examining the middle tract, $C_4AC_4TC_3G$, yields the strongest and most selective 490 nm band in comparison with its shorter $C_4AC_3TC_3G$ and longer $C_4AC_5TC_3G$ counterparts (Figure

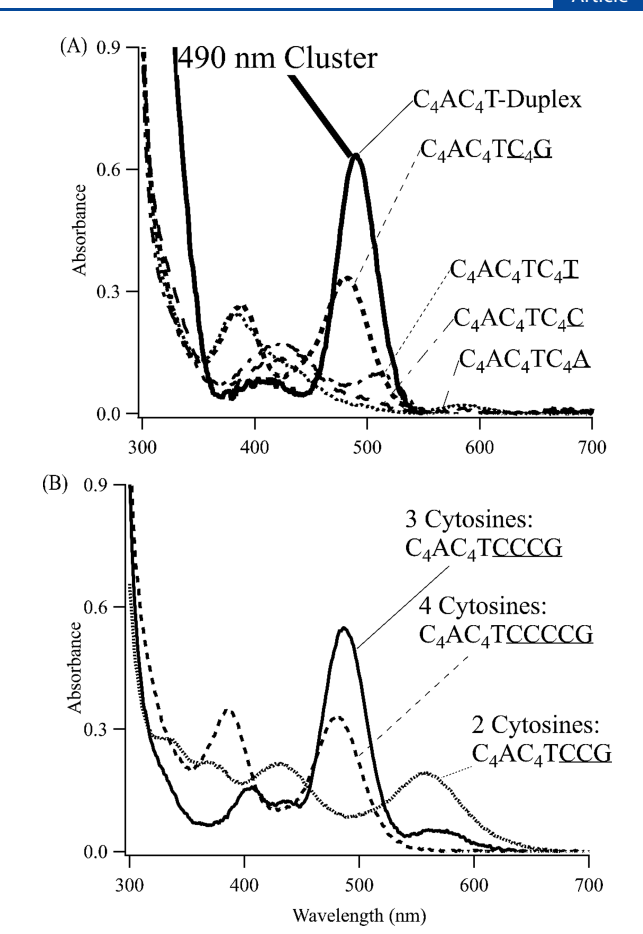


Figure 1. (A) Absorption spectra showing that both the C₄AC₄T-duplex and single-stranded C₄AC₄TC₄G produce the target cluster with $\lambda=490$ nm, whereas C₄AC₄TC₄X (X = T, C, and A) does not yield this species. (B) In relation to the shorter C₄AC₄TC₂G (dotted line) and longer C₄AC₄TC₄G (dashed line), C₄AC₄TC₃G (solid line) yields the strongest A₄₉₀.

S2A). For the first tract, the DNA strands have a threshold length needed to support the cluster (Figure S2B). While $\underline{C_3A}C_4TC_3G$ reduces the 490 nm absorption, $\underline{C_4A}C_4TC_3G$ and $\underline{C_5A}C_4TC_3G$ yield comparably strong peaks. Therefore, the minimal $C_4AC_4TC_3G$ sequence was used to understand the binding site for the 490 nm cluster.

Within the tracts, cytosines were eliminated or replaced to probe the coordination environment. First, cytosines were eliminated to create abasic sites in the polymer template (Figure 2A). Single cytosines in the first and second tracts were replaced with a uracil that was enzymatically excised, and neither modified strand produces the 490 nm cluster. Second, cytosines were replaced with thymines that are weaker ligands (Figure S3). At neutral pH, the N3 of thymine is protonated, which quenches cluster emission, whereas the corresponding N3 in cytosine is deprotonated, which favors fluorescent silver chromophores. 39,40 Cytosine—thymine substitutions in each of the three tracts of C₄AC₄TC₃G yield the same outcome—a 400 nm band supplants the 490 nm absorption. Thus, either eliminating a cytosine or substituting it with a poorer ligand disfavors the 490 nm cluster. Because single cytosine changes elicit these dramatic spectral changes, we suggest that a network of contiguous cytosines coordinate the 490 nm absorbing cluster.

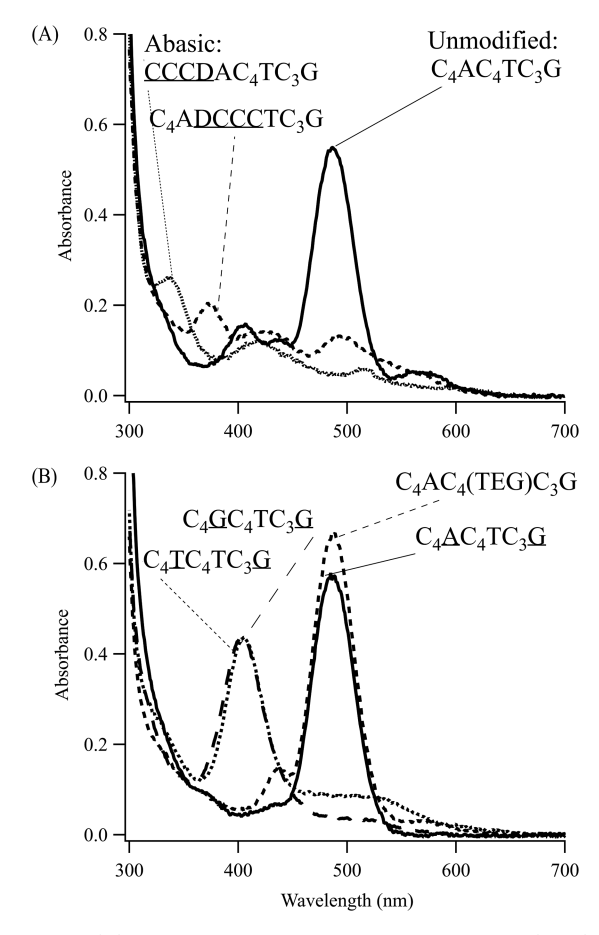


Figure 2. (A) Absorption spectra using $C_4AC_4TC_3G$ (solid) vs strands with abasic sites in the first (dotted) and second (dashed) tracts, as indicated by D. (B) Absorption spectra of $C_4AC_4TC_3G$ vs different combinations of nucleobases in the first tract ($C_4TC_4TC_3G$ [dotted] and $C_4GC_4TC_3G$ [dashed]). The specific changes are underlined. Additionally, the strong absorption with $C_4AC_4(TEG)$ - C_3G is highlighted in relation to $C_4AC_4TC_3G$.

Terminating Nucleobases. Each cytosine tract terminates with a different nucleobase with a distinct role. We first consider the thymine. This nucleobase can be replaced with a guanine or adenine but not with cytosine, which forms a competing 400 nm cluster (Figure S4). This alternate species underscores the need to segregate cytosine tracts to favor the 490 nm cluster. This site in the polymer can accommodate more drastic modifications. The thymine nucleobase was eliminated, and this sequence with an abasic site still produces the 490 nm cluster with even stronger absorbance (Figure S5). This enhanced absorption sharply contrasts with the 490 nm absorption band that is extinguished due to abasic sites in the cytosine tracts and thus further supports the chemical differences between the cytosines and the thymine (Figures 2A vs S5). Beyond DNA-related changes, the entire thymine nucleotide can be replaced with a triethylene glycol (TEG) linker while maintaining the 490 nm absorption band (Figure 2B). Because both the abasic site and triethylene glycol are flexible, we suggest that the thymine site is a junction in a folded oligonucleotide.

In contrast with the interchangeable thymine, the terminal adenine in the first tract and guanine in the third tract are an exclusive pair that favor the 490 nm cluster. These nucleobases were identified from the nine sequences $C_4XC_4TC_3Z$ with X

and Z individually being adenine, thymine, or guanine (Figures 2B and S6). The sequence with X = A and Z = G selectively develops the target cluster with the strongest absorption band at 490 nm. These nucleobases may be a coupled pair because they may be proximal in a folded $C_4AC_4TC_3G$ (see Figure 3 insets).

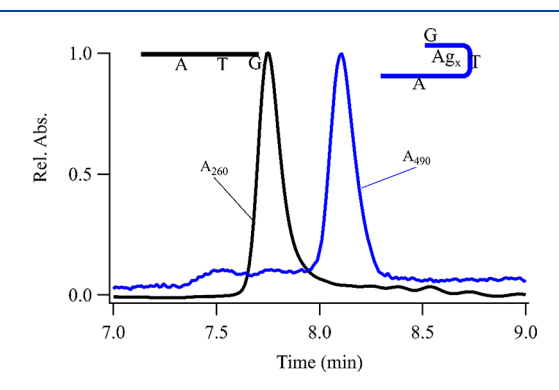


Figure 3. Size exclusion chromatograms of native $C_4AC_4TC_3G$ measured at 260 nm (black) and of the $C_4AC_4TC_3G$ —cluster complex measured at 490 nm (blue). The latter complex elutes later and is thus more compact than the native DNA. The inset cartoons suggest a more compact shape for the DNA—cluster (Ag_x) complex relative to the native strand.

Secondary Structure—Cluster Condenses DNA. The secondary structure of C₄AC₄TC₃G is changed by the cluster, and chromatography and fluorescence studies show that the native DNA condenses around the cluster. Size exclusion chromatography typically resolves DNA strands based on their strand length and hydrodynamic radii, but this relationship is altered by silver clusters that fold and assemble DNA strands. 34,43,57,59 For C₄AC₄TC₃G, the cluster conjugate elutes later and is thus more compact than its unligated counterpart (Figure 3). These size changes were gauged against a set of thymine oligonucleotides (Figure S7). Apo-C₄AC₄TC₃G elutes as a dT₁₃, which is similar to its overall length of 14 nucleotides. Thus, the uncomplexed DNA strand behaves as a random coil polymer like the oligothymines. 60 In contrast, the ligated strand elutes later because it has a 17% smaller hydrodynamic radius than that for the native strand. A change in DNA shape was also examined in situ by fluorescence correlation spectroscopy (FCS). Two-focus FCS measures crossing times between two laterally shifted laser foci and thereby determines diffusion coefficients for fluorescent DNA strands.⁵⁵ A fluorescein-tagged C₄AC₄TC₃G and the C₄AC₄TC₃G-cluster conjugate have diffusion coefficients of 118 \pm 3 and 140 \pm 7 μ m²/s, respectively, so the cluster conjugate has an ~15% smaller hydrodynamic radius than that of the native fluorescein-DNA. Fluorescence anisotropy further interrogated the DNA shape via rotational correlation times. The native C₄AC₄TC₃G was sparsely labeled with the noncovalently bound dye SYBR Gold, and its rotational correlation time of 2.2 ± 0.1 ns is consistent with earlier studies of single-stranded 15-mer oligonucleotides. 61,62 The cluster-laden strand has a shorter rotational correlation time of 1.6 \pm 0.1 ns, which translates to an ~11% drop in the hydrodynamic radius based on a spherical shape. Taken together, these chromatography and fluorescence studies show that C₄AC₄TC₃G changes from a random coil to a more condensed and presumably more organized secondary

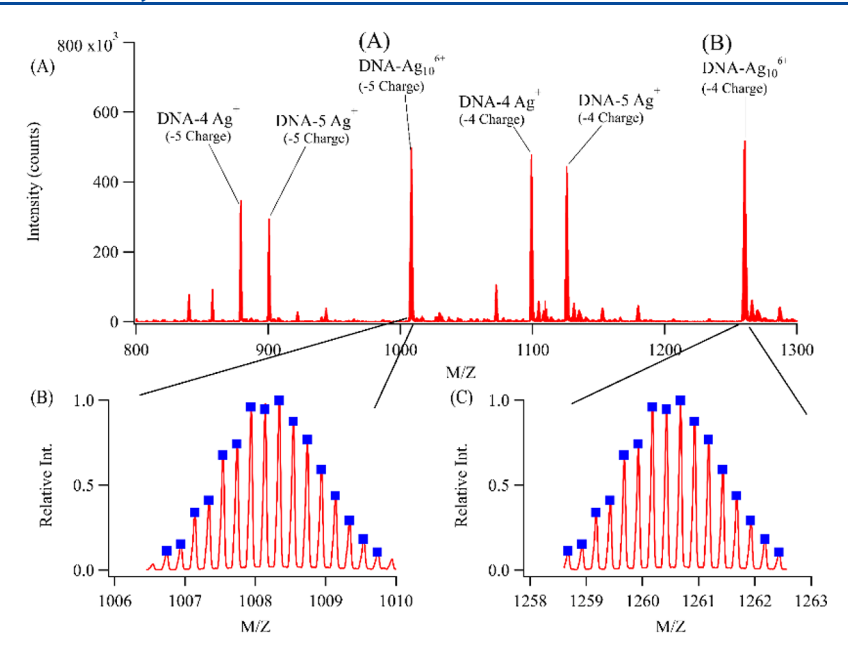


Figure 4. (A) Mass:charge spectrum of a $C_4AC_4(TEG)C_3G$ complex with 4, 5, and 10 silvers. (B and C) Expanded view of the complexes with overall charges of -5 and -4, respectively. The blue tick marks represent the predicted masses based on the following molecular formulas $C_{125}H_{159}O_{81}N_{43}P_{13}Ag_{10}^{-5}$ (B) and $C_{125}H_{160}O_{81}N_{43}P_{13}Ag_{10}^{-4}$ (C). The precisions between the observed and predicted masses of the isotopologues are 1.7 ± 0.2 ppm (B) and 1.7 ± 0.2 ppm (C).

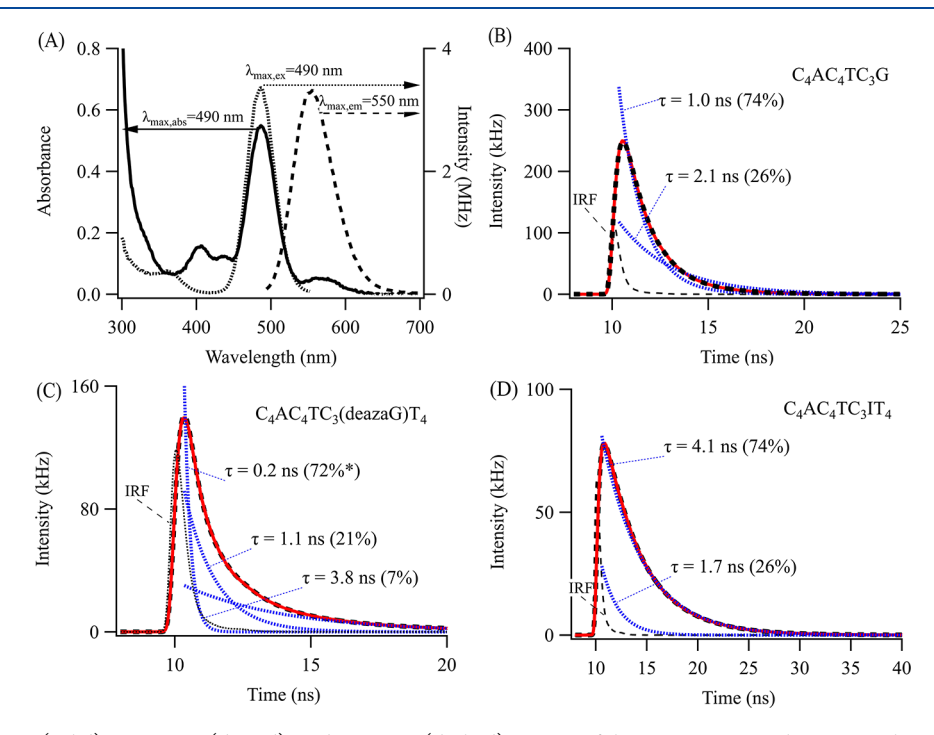


Figure 5. (A) Absorption (solid), excitation (dotted), and emission (dashed) spectra of the $C_4AC_4TC_3G$ -cluster complex. Time-resolved emission decays for the (B) $C_4AC_4TC_3G$ -, (C) $C_4AC_4TC_3(deazaG)T_4$ -, and (D) $C_4AC_4TC_3IT_4$ -cluster complexes (red) with models (black dashes) based on single exponential decays (blue dots) reconvoluted with the IRF (black dashes). The time constants and the relative amplitudes of the exponential decays are provided. The * in part C indicates that the amplitude of the fast decay is scaled down by 2.

structure when bound to the cluster and that the oligonucleotide appears to fold at the flexible thymine site.

Adenine and Guanine Are Crucial to Forming the Ag₁₀⁶⁺ Fluorophore. C₄AC₄TC₃G develops a specific silver molecule whose stoichiometry and charge were determined by mass spectrometry (Figures 4 and S8). The analogous triethylene glycol linked strand C₄AC₄(TEG)C₃G also forms this cluster and was used because its cluster conjugate best

survives purification via dilution and dialysis. This complex was then studied by electrospray ionization mass spectrometry to determine the cluster stoichiometry and charge. 33,43,63 This strand preferentially binds 4, 5, and 10 silvers, and these stoichiometries are consistent with the molecular clusters identified in previous reports. 46,52,53 These complexes are distinguished by their oxidation states, which were derived from the isotope fine structure within the M/Z peaks (Figures

Table 1. Lifetimes and Fluorescence Quantum Yields of Silver Clusters Bound to C4XC4TC3G Sequences

X in C ₄ XC ₄ TC ₃ G	Lifetimes ^a	Quantum Yield ^{a,b}
NH ₂ NH ₂ NH ₂ Adenine	$ au_1 = 1.12 \pm 0.15 \text{ ns}$ $(70 \pm 5\%)$ $ au_2 = 2.14 \pm 0.08 \text{ ns}$ $(30 \pm 5\%)$	$\phi_f = 19 \pm 2$
NH(CH ₃) N N N 6-methyladenine	$\tau_1 = 1.09 \pm 0.05 \text{ ns}$ $(44 \pm 12\%)$ $\tau_2 = 2.32 \pm 0.05 \text{ ns}$ $(56 \pm 12\%)$	$\phi_f = 21 \pm 2$
N NH ₂	$ au_1 = 1.14 \pm 0.01 \text{ ns}$ $(66 \pm 3\%)$ $ au_2 = 2.26 \pm 0.03 \text{ ns}$ $(34 \pm 3\%)$	$\phi_f = 21 \pm 2$
2-aminopurine NH2 N N 7-deazaadenine	$\tau_1 = 0.48 \pm 0.07 \text{ ns}$ $(54 \pm 16\%)$ $\tau_2 = 1.08 \pm 0.14 \text{ ns}$ $(43 \pm 14\%)$ $\tau_3 = 2.53 \pm 0.55 \text{ ns}$ $(3 \pm 2\%)$	$\phi_f = 11 \pm 1$

[&]quot;Averages and standard deviations from three or more measurements with different samples. ^bQuantum yields measured using fluorescein as a standard. ⁷⁹

4B,C and S8). These distributions are set by the molecular formulas with their natural mixtures of isotopes, and we are particularly interested in the H⁺ because it changes with the charges of the cluster adducts. The DNA complexes with four and five silvers have four and five fewer H⁺, respectively, than the native oligonucleotide, so these silvers are completely oxidized and thus optically silent. In contrast, the strands with 10 silvers have 6 Ag⁺ and 4 Ag⁰, and Ag₁₀ are optical chromophores. Thus, we assign this Ag₁₀ cluster within the $C_4AC_4(TEG)C_3G$ and related strands to be the λ = 490 nm chromophore in these studies.

This $^{1}\text{Ag}_{10}^{6+}$ adduct emits with $\lambda_{\text{em,max}}=540$ nm when excited with $\lambda_{\text{ex,max}}=490$ nm (Figure 5A). The excitation and absorption maxima match, which indicates that a single emissive species is preferred. This fluorescence has a quantum yield of 19 \pm 2% and a biexponential decay with lifetimes of 1.1 ± 0.2 and 2.1 ± 0.1 ns and relative amplitudes of $70 \pm 5\%$ and $30 \pm 5\%$, respectively (Figure 5B and Table 1). These measurements are consistent with the fluorescence quantum yields of 0.2-40% and lifetimes of 0.2-4 ns for other green emitting silver cluster–DNA conjugates. 31,47,65 This cluster also exhibits circular dichroism with $\varepsilon_{\min}=490$ nm, which also

matches the absorption maximum (Figure S9). This correspondence suggests that the cluster is bound by the chiral $C_4AC_4TC_3G$ template, and the degree of DNA coordination is gauged by the anisotropy, κ , which measures the inherent circular dichroism by normalizing the ellipticity based on the absorbance. The κ of 0.3 \times 10⁻³ has been reported for related DNA–silver cluster complexes and suggests that the cluster binds in a similar coordination environment. The suggestion of the suggestion of the cluster binds in a similar coordination environment.

The coordination environment for the cluster directly depends on the adenine and guanine, and derivatives of these nucleobases alter the cluster photophysics. The variants of adenine were 2-aminopurine, 6-methyladenine, and 7-deazaadenine, and the guanine analogues were 8-bromoguanine, inosine, and 7-deazaguanine (Tables 1 and 2 and Figures S10 and S11). These nucleobases behave like their natural counterparts and produce clusters with $\lambda \sim 490$ nm, although the cluster yields varied. However, fluorescence quantum yields and lifetimes are inherent quantities and do not depend on the chromophore concentration. Clusters made in oligonucleotides with 2-aminopurine and 6-methyladenine behave similarly to those with adenine, yielding biexponential decays with

Table 2. Lifetimes and Fluorescence Quantum Yields of Silver Clusters Bound to C₄AC₄TC₃YT₄ Sequences

Y in C ₄ AC ₄ TC ₃ YT ₄	Lifetimes ^a	Quantum Yield ^{a,b}
Ĭ	$\tau_1 = 1.5 \pm 0.4 \text{ ns}$ $(67 \pm 4\%)$	$\phi_f = 25 \pm 5$
ŅH	$\tau_2 = 2.7 \pm 0.2 \text{ ns}$	
	$(33 \pm 4\%)$	
NH ₂	,	
Guanine		
0	$\tau_1=1.3\pm0.3~ns$	$\varphi_f = 24 \pm 3$
N NH	$(64 \pm 12\%)$	
Br——	$\tau_2 = 2.6 \pm 0.2 \text{ ns}$	
N NH ₂	$(36 \pm 12\%)$	
8-Bromoguanine		
Q	$\tau_1 = 0.22 \pm 0.04 \text{ ns}$	$\phi_{\rm f} = 1 \pm 0.5$
	$(75 \pm 6\%)$	$\psi_1 - 1 \pm 0.5$
NH	$\tau_2 = 1.4 \pm 0.2 \text{ ns}$	
	$(16 \pm 4\%)$	
N NH ₂	$\tau_3 = 3.8 \pm 0.2 \text{ ns}$	
7-deazaguanine	$(9 \pm 3\%)$	
O.	$\tau_1 = 1.5 \pm 0.2 \text{ ns}$	$\phi_f = 63 \pm 2$
	$(25 \pm 1\%)$	$\psi_1 OS \perp Z$
N	$\tau_2 = 4.0 \pm 0.1 \text{ ns}$	
	$(75 \pm 1\%)$	
N N		
Inosine		

[&]quot;Averages and standard deviations from three or more measurements with different samples. ^bQuantum yields measured using fluorescein as a standard. ⁷⁹

lifetimes of \sim 1.1 and \sim 2.3 ns and fluorescence quantum yields of \sim 20%. However, 7-deazaadenine suppresses the cluster emission \sim 2-fold and opens a new fluorescence decay pathway with an \sim 0.5 ns lifetime. The guanine derivatives produce larger changes (Figure 5C,D). For these studies, $C_4AC_4TC_3ZT_4$ strands were used because they are commercially available and produce clusters with fluorescence quantum yields and lifetimes that are similar to those in $C_4AC_4TC_3G$ (Table 1). Although clusters with guanine and 8-bromoguanine behave similarly, clusters with 7-deazaguanine and inosine are distinct with 1 and 63% quantum yields and dominant lifetimes that are 0.2 and 4.0 ns, respectively. These differences may arise because of electron transfer between the photoexcited cluster and the DNA nucleobases, as subsequently discussed.

DISCUSSION

The sequence and structure of $C_4AC_4TC_3G$ selectively develop the Ag_{10}^{6+} chromophore with $\lambda_{\rm ex}/\lambda_{\rm em}=490/540$ nm. Our studies identified three types of nucleobase ligands within the

coordination environment, and we now discuss how they control the structure of the DNA host and the spectra of the cluster adduct.

Consecutive Cytosines and Multidentate Coordination. Cytosine dominates this sequence with 11 of the 14 nucleobases, but they must be separated to avoid a mixture of clusters (Figure S4). 39,67 We suggest that the three cytosine tracts in C₄AC₄TC₃G are collective subunits. When only a single cytosine is eliminated or replaced in any of the tracts, the 490 nm absorption is extinguished, so the cluster binding site is compromised (Figures 2A and S3). Thus, the cytosines act together, as observed for other silver cluster templates. For example, (C₂A)₆ selectively develops a violet Ag₁₀⁶⁺ cluster, whereas its permuted analogue (CAC)₆ shifts the absorption and quenches the emission of its cluster adducts.⁵¹ This permuted strand recovers the strong spectra by appending a 5' cytosine, which presumably restores the necessary number of six CC pairs. Other sequences with consecutive cytosines have also been identified. 34,42,68 We suggest such cytosine tracts are multidentate ligands that coordinate multiple silvers. A single

cytosine preferentially binds silver via its deprotonated N3, so repeated cytosines could bind multiple silvers. Consequently, the cluster adduct would be dispersed along the DNA contour, as supported by two observations. First, two Ag₁₀⁶⁺ clusters with distinct emission and structures have been studied by X-ray absorption spectroscopy. 52,53 The fluorescent species is distinguished by its relatively high silver nucleobase and low silver-silver coordination numbers that support a highly coordinated cluster. We therefore suggest that nucleobase ligands in an oligonucleotide imprint the shape of their cluster adducts, as observed for noble metal-thiolate complexes. 17,69 Second, different types of silver clusters with different numbers of Ag⁰ have been identified by mass spectrometry. 33,52,70,71 Their distinct spectra can be explained on the basis of elongated clusters that balance coordination by multiple nucleobases vs Ag⁰-Ag⁰ bonding. Therefore, we propose that the cytosine tracts in C₄AC₄TC₃G are multidentate ligands that partially guide cluster geometries along the contours of the DNA scaffold.

Interchangeable Thymine and Folded DNA. The thymine acts as a neutral site within the overall polymer because it can be interchanged not only with other nucleobases but also with abasic and triethylene glycol linkers (Figures S5 and 2B). Because these latter modifications are flexible, we suggest that this site is a junction that allows Ag_{10}^{6+} to fold its host (Figure 3). ^{72,73} Prior X-ray spectroscopy studies establish that Ag⁺ and Ag⁰ within a cluster segregate and thus have different functions. ^{52,53} Specifically, we suggest that Ag⁺ linearly coordinates nucleobases and cross-links nucleobases in remote parts of a DNA oligomer, as previously suggested for $(C_2X)_6$ -cluster complexes. $(C_2A)_6$ and $(C_2T)_6$ are strands with a minimal length that can support a ${\rm Ag_{10}}^{6+}$ cluster, and the six Ag+ in the cluster may form C-Ag+-C metallo-base pairs that intramolecularly pull the strand together. Thus, these results suggest that the thymine in C₄AC₄TC₃G indirectly controls the coordination environment because the strand folds at this site. This folded structure may control the relative positions of the other two terminating nucleobases.

Terminating Nucleobases and Electronic Environ**ment.** The adenine/guanine pairs in $C_4AC_4TC_3G$ are the only ligands that selectively develop the cluster, and derivatives of these nucleobases control the electronic environment of the clusters (Tables 1 and 2). Among the adenine derivatives, 7deazaadenine is distinct because its fluorescence decay favors a shorter lifetime of ~0.5 ns and has a 2-fold lower fluorescence quantum yield. The guanine derivatives show greater variation. From inosine to 7-dezaguanine, the fluorescence quantum yield drops 60-fold and the time constant for the dominant component of the fluorescence decay falls by 3.8 ns. Thus, modified nucleobases reveal a new way to control silver cluster emission that complements variations in DNA sequence and structure. A possible mechanism for these fluorescence changes may be electron transfer from the nucleobases to the embedded silver clusters. For the nucleobases 7-deazaguanine, 7-dezadenine, guanine, and inosine, the oxidation potentials increase in the order 1.0, 1.3, 1.3, and 1.5 V vs. NHE. Our studies correspondingly find that the fluorescence quantum yields and lifetimes of the cluster adducts increase. To understand this correlation more thoroughly, the relative energies of the electronic states of the cluster and nucleobases are needed. 77 As a key first step, prior studies establish that the silver clusters are electronically coupled to nucleobases, as they

emit when the nucleobases are optically excited.⁷⁸ In addition, electronically excited clusters reduce cytosine, as supported by transient absorption spectra of the cytosine anion.³⁶ Our studies suggest that the 490 nm cluster photooxidizes the nucleobases, and it may act differently because molecular silver clusters have widely ranging redox potentials.²⁷ Thus, different clusters may control the direction of electron transfer with their DNA host, a possibility that we are now considering.

CONCLUSION

DNA strands coordinate molecular silver clusters via their nucleobases. Our studies identify distinct roles for the nucleobases in the $\rm C_4AC_4TC_3G-Ag_{10}^{6+}$ complex. The cytosine tracts collectively stabilize the cluster. The thymine is a flexible junction within a folded strand. The adenine and guanine specifically form the $\lambda=490$ nm cluster and control the photophysics of this adduct. Importantly, the heteroatoms within these nucleobases influence the fluorescence lifetimes and quantum yields of the cluster chromophores. Thus, modified nucleobases could expand the code of DNA sequences that control not only the spectra but also the brightness of a silver cluster chromophore.

ASSOCIATED CONTENT

Supporting Information

The Supporting Information is available free of charge on the ACS Publications website at DOI: 10.1021/acs.jpcc.8b09414.

Eleven figures related to the DNA–cluster complexes. These describe absorption spectra with the C_4AC_4T d u p l e x a n d C $_4$ A C $_4$ T a l o n e , w i t h $C_4AC_4TC_3G$ derivatives with different numbers of cytosines in the three tracts, with stands with thymines that interrupt the cytosine tracts, with $C_4AC_4YC_3G$ strands with $Y=G,\,T,\,A,\,$ and $C,\,$ with strands with the thymine and an abasic site, and with the nine possible combinations of $C_4XC_4TC_3Z$ strands; size exclusion chromatograms of $C_4AC_4TC_3G$ without and with the cluster and of the thymine standards; mass spectra of the $C_4AC_4(TEG)C_3G$ complexes with 4 and 5 Ag^+ and with Ag_{10}^{6+} ; circular dichroism spectra of the $C_4AC_4TC_3G$ –cluster complex; and absorption spectra of $C_4XC_4TC_3G$ derivatives and of $C_4AC_4TC_3ZT_4$ derivatives (PDF)

AUTHOR INFORMATION

Corresponding Author

*E-mail: jeff.petty@furman.edu. Phone: 864-294-2689.

ORCID ®

Jeffrey T. Petty: 0000-0003-0149-5335 Mainak Ganguly: 0000-0002-5315-7381 Chen He: 0000-0001-5426-769X

Chell Tie: 0000-0001-3420-769X

Robert M. Dickson: 0000-0003-0042-6194

Author Contributions

The manuscript was written through contributions of all authors. All authors have given approval to the final version of the manuscript.

Author Contributions

J.T.P., M.G.: These authors contributed equally.

Funding

We thank the National Science Foundation (CHE-1611451), National Institutes of Health (1R15GM102818), and the Furman Advantage program. This work was supported in part by the National Science Foundation EPSCoR Program under NSF Award No. OIA-1655740. Any opinions, findings and conclusions or recommendations expressed in this material are those of the author(s) and do not necessarily reflect those of the National Science Foundation. This work was also performed, in part, at the Center for Integrated Nanotechnologies, an Office of Science User Facility operated for the U.S. Department of Energy (DOE) Office of Science. Los Alamos National Laboratory, an affirmative action equal opportunity employer, is operated by Los Alamos National Security, LLC, for the National Nuclear Security Administration of the U.S. DOE under contract DE-AC52-06NA25396.

Notes

The authors declare no competing financial interest.

ACKNOWLEDGMENTS

We are grateful to C. Edmunds for maintenance of the mass spectrometer. We thank Jörg Enderlein for the MATLAB routines used to analyze the two-focus FCS data. We are grateful to the National Science Foundation and the National Institutes of Health for support of this work.

REFERENCES

- (1) Kittel, C. Introduction to Solid State Physics, 8th ed.; Wiley: 2004; p 704.
- (2) Kubo, R.; Kawabata, A.; Kobayashi, S.-i. Electronic Properties of Small Particles. Annu. Rev. Mater. Sci. 1984, 14, 49-66.
- (3) Jain, P. K.; Huang, X.; El-Sayed, I. H.; El-Sayed, M. A. Noble Metals on the Nanoscale: Optical and Photothermal Properties and Some Applications in Imaging, Sensing, Biology, and Medicine. Acc. Chem. Res. 2008, 41, 1578-86.
- (4) Gimeno, M. C. The Chemistry of Gold. In Modern Supramolecular Gold Chemistry; Laguna, A., Ed.; Wiley-VCH: 2009.
- (5) Gell, L.; Kulesza, A.; Petersen, J.; Röhr, M. I. S.; Mitrić, R.; Bonačić-Koutecký, V. Tuning Structural and Optical Properties of Thiolate-Protected Silver Clusters by Formation of a Silver Core with Confined Electrons. J. Phys. Chem. C 2013, 117, 14824-14831.
- (6) Han, B. Y.; Wang, E. K. DNA-Templated Fluorescent Silver Nanoclusters. Anal. Bioanal. Chem. 2012, 402, 129-138.
- (7) Obliosca, J. M.; Liu, C.; Batson, R. A.; Babin, M. C.; Werner, J. H.; Yeh, H.-C. DNA/Rna Detection Using DNA-Templated Few-Atom Silver Nanoclusters. Biosensors 2013, 3, 185-200.
- (8) Petty, J. T.; Story, S. P.; Hsiang, J. C.; Dickson, R. M. DNA-Templated Molecular Silver Fluorophores. J. Phys. Chem. Lett. 2013,
- (9) Liu, J. DNA-Stabilized, Fluorescent, Metal Nanoclusters for Biosensor Development. TrAC, Trends Anal. Chem. 2014, 58, 99-
- (10) Zheng, K.; Yuan, X.; Goswami, N.; Zhang, Q.; Xie, J. Recent Advances in the Synthesis, Characterization, and Biomedical Applications of Ultrasmall Thiolated Silver Nanoclusters. RSC Adv. 2014, 4, 60581-60596.
- (11) Gwinn, E.; Schultz, D.; Copp, S.; Swasey, S. DNA-Protected Silver Clusters for Nanophotonics. Nanomaterials 2015, 5, 180-207.
- (12) Bonacic-Koutecky, V.; Veyret, V.; Mitric, R. Ab Initio Study of the Absorption Spectra of Ag_n (N = 5-8) Clusters. J. Chem. Phys. 2001, 115, 10450-10460.
- (13) de Heer, W. A. The Physics of Simple Metal Clusters: Experimental Aspects and Simple Models. Rev. Mod. Phys. 1993, 65, 611 - 676.
- (14) Hakkinen, H.; Walter, M.; Gronbeck, H. Divide and Protect: Capping Gold Nanoclusters with Molecular Gold-Thiolate Rings. J. Phys. Chem. B 2006, 110, 9927-9931.
- (15) Yumura, T.; Kumondai, M.; Kuroda, Y.; Wakasugi, T.; Kobayashi, H. Utilizing Super-Atom Orbital Ideas to Understand

- Properties of Silver Clusters inside Zsm-5 Zeolite. RSC Adv. 2017, 7, 4950-4959.
- (16) Hakkinen, H. The Gold-Sulfur Interface at the Nanoscale. Nat. Chem. 2012, 4, 443-455.
- (17) Chen, Y.; Liu, C.; Tang, Q.; Zeng, C.; Higaki, T.; Das, A.; Jiang, D.-e.; Rosi, N. L.; Jin, R. Isomerism in Au₂₈(Sr)₂₀ Nanocluster and Stable Structures. J. Am. Chem. Soc. 2016, 138, 1482-1485.
- (18) Taylor, M. G.; Mpourmpakis, G. Thermodynamic Stability of Ligand-Protected Metal Nanoclusters. Nat. Commun. 2017, 8, 15988.
- (19) Qian, H.; Zhu, M.; Wu, Z.; Jin, R. Quantum Sized Gold Nanoclusters with Atomic Precision. Acc. Chem. Res. 2012, 45, 1470-
- (20) Desireddy, A.; Conn, B. E.; Guo, J.; Yoon, B.; Barnett, R. N.; Monahan, B. M.; Kirschbaum, K.; Griffith, W. P.; Whetten, R. L.; Landman, U.; et al. Ultrastable Silver Nanoparticles. Nature 2013, 501, 399-402.
- (21) Yang, H.; Wang, Y.; Huang, H.; Gell, L.; Lehtovaara, L.; Malola, S.; Häkkinen, H.; Zheng, N. All-Thiol-Stabilized Ag₄₄ and Au₁₂ag₃₂ Nanoparticles with Single-Crystal Structures. Nat. Commun. 2013, 4,
- (22) Petty, J. T.; Zheng, J.; Hud, N. V.; Dickson, R. M. DNA-Templated Ag Nanocluster Formation. J. Am. Chem. Soc. 2004, 126, 5207-12.
- (23) Petty, J. T.; Sengupta, B.; Story, S. P.; Degtyareva, N. N. DNA Sensing by Amplifying the Number of near-Infrared Emitting, Oligonucleotide-Encapsulated Silver Clusters. Anal. Chem. 2011, 83,
- (24) Yeh, H. C.; Sharma, J.; Han, J. J.; Martinez, J. S.; Werner, J. H. A DNA-Silver Nanocluster Probe That Fluoresces Upon Hybridization. Nano Lett. 2010, 10, 3106-10.
- (25) Choi, S.; Yu, J.; Patel, S. A.; Tzeng, Y.-L.; Dickson, R. M. Tailoring Silver Nanodots for Intracellular Staining. Photochem. Photobiol. Sci. 2011, 10, 109-115.
- (26) Yu, J.; Patel, S. A.; Dickson, R. M. In Vitro and Intracellular Production of Peptide-Encapsulated Fluorescent Silver Nanoclusters. Angew. Chem., Int. Ed. 2007, 46, 2028-2030.
- (27) Henglein, A.; Mulvaney, P.; Linnert, T. Chemistry of Agn Aggregates in Aqueous-Solution - Nonmetallic Oligomeric Clusters and Metallic Particles. Faraday Discuss. 1991, 92, 31-44.
- (28) Zheng, J.; Petty, J. T.; Dickson, R. M. High Quantum Yield Blue Emission Form Water-Soluble Au8 Nanodots. J. Am. Chem. Soc. 2003, 125, 7780-7781.
- (29) Gwinn, E. G.; O'Neill, P.; Guerrero, A. J.; Bouwmeester, D.; Fygenson, D. K. Sequence-Dependent Fluorescence of DNA-Hosted Silver Nanoclusters. Adv. Mater. (Weinheim, Ger.) 2008, 20, 279-283.
- (30) Jensen, R. H.; Davidson, N. Spectrophotometric, Potentiometric, and Density Gradient Ultracentrifugation Studies of the Binding of Silver Ion by DNA. Biopolymers 1966, 4, 17-32.
- (31) Richards, C. I.; Choi, S.; Hsiang, J.-C.; Antoku, Y.; Vosch, T.; Bongiorno, A.; Tzeng, Y.-L.; Dickson, R. M. Oligonucleotide-Stabilized Ag Nanocluster Fluorophores. J. Am. Chem. Soc. 2008, 130, 5038-5039.
- (32) Lavis, L. D.; Raines, R. T. Bright Ideas for Chemical Biology. ACS Chem. Biol. 2008, 3, 142-155.
- (33) Schultz, D.; Gardner, K.; Oemrawsingh, S. S. R.; Markešević, N.; Olsson, K.; Debord, M.; Bouwmeester, D.; Gwinn, E. Evidence for Rod-Shaped DNA-Stabilized Silver Nanocluster Emitters. Adv. Mater. (Weinheim, Ger.) 2013, 25, 2797-2803.
- (34) Petty, J. T.; Giri, B.; Miller, I. C.; Nicholson, D. A.; Sergev, O. O.; Banks, T. M.; Story, S. P. Silver Clusters as Both Chromophoric Reporters and DNA Ligands. Anal. Chem. 2013, 85, 2183-2190.
- (35) Tyagi, S.; Kramer, F. R. Molecular Beacons: Probes That Fluoresce Upon Hybridization. Nat. Biotechnol. 1996, 14, 303-308.
- (36) Patel, S. A.; Cozzuol, M.; Hales, J. M.; Richards, C. I.; Sartin, M.; Hsiang, J.-C.; Vosch, T.; Perry, J. W.; Dickson, R. M. Electron Transfer-Induced Blinking in Ag Nanodot Fluorescence. J. Phys. Chem. C 2009, 113, 20264-20270.

- (37) Hsiang, J.-C.; Fleischer, B. C.; Dickson, R. M. Dark State-Modulated Fluorescence Correlation Spectroscopy for Quantitative Signal Recovery. *J. Phys. Chem. Lett.* **2016**, *7*, 2496–2501.
- (38) Krause, S.; Carro-Temboury, M. R.; Cerretani, C.; Vosch, T. Anti-Stokes Fluorescence Microscopy Using Direct and Indirect Dark State Formation. *Chem. Commun.* **2018**, *54*, 4569–4572.
- (39) Ritchie, C. M.; Johnsen, K. R.; Kiser, J. R.; Antoku, Y.; Dickson, R. M.; Petty, J. T. Ag Nanocluster Formation Using a Cytosine Oligonucleotide Template. *J. Phys. Chem. C* **2007**, *111*, 175–181.
- (40) Sengupta, B.; Ritchie, C. M.; Buckman, J. G.; Johnsen, K. R.; Goodwin, P. M.; Petty, J. T. Base-Directed Formation of Fluorescent Silver Clusters. *J. Phys. Chem. C* **2008**, *112*, 18776–18782.
- (41) Lippert, B.; Sanz Miguel, P. J. The Renaissance of Metal—Pyrimidine Nucleobase Coordination Chemistry. *Acc. Chem. Res.* **2016**, 49, 1537–1545.
- (42) Copp, S. M.; Bogdanov, P.; Debord, M.; Singh, A.; Gwinn, E. Base Motif Recognition and Design of DNA Templates for Fluorescent Silver Clusters by Machine Learning. *Adv. Mater.* (Weinheim, Ger.) 2014, 26, 5839–5845.
- (43) Petty, J. T.; Sergev, O. O.; Kantor, A. G.; Rankine, I. J.; Ganguly, M.; David, F. D.; Wheeler, S. K.; Wheeler, J. F. Ten-Atom Silver Cluster Signaling and Tempering DNA Hybridization. *Anal. Chem.* **2015**, *87*, 5302–5309.
- (44) Driehorst, T.; O'Neill, P.; Goodwin, P. M.; Pennathur, S.; Fygenson, D. K. Distinct Conformations of DNA-Stabilized Fluorescent Silver Nanoclusters Revealed by Electrophoretic Mobility and Diffusivity Measurements. *Langmuir* 2011, 27, 8923–8933.
- (45) Fleischer, B. C.; Petty, J. T.; Hsiang, J.-C.; Dickson, R. M. Optically Activated Delayed Fluorescence. *J. Phys. Chem. Lett.* **2017**, *8*, 3536–3543.
- (46) Copp, S. M.; Schultz, D.; Swasey, S.; Pavlovich, J.; Debord, M.; Chiu, A.; Olsson, K.; Gwinn, E. Magic Numbers in DNA-Stabilized Fluorescent Silver Clusters Lead to Magic Colors. *J. Phys. Chem. Lett.* **2014**, *5*, 959–963.
- (47) Sharma, J.; Yeh, H. C.; Yoo, H.; Werner, J. H.; Martinez, J. S. A Complementary Palette of Fluorescent Silver Nanoclusters. *Chem. Commun.* **2010**, *46*, 3280–2.
- (48) Petty, J. T.; Fan, C.; Story, S. P.; Sengupta, B.; Sartin, M.; Hsiang, J.-C.; Perry, J. W.; Dickson, R. M. Optically Enhanced, near-Ir, Silver Cluster Emission Altered by Single Base Changes in the DNA Template. *J. Phys. Chem. B* **2011**, *115*, 7996–8003.
- (49) Bloomfield, V. A.; Crothers, D. M.; Tinoco, I. *Nucleic Acids: Structures, Properties, and Functions*; University Science Books: Sausalito, CA, 2000; Chapter 14, p 794.
- (50) Petty, J. T.; Story, S. P.; Juarez, S.; Votto, S. S.; Herbst, A. G.; Degtyareva, N. N.; Sengupta, B. Optical Sensing by Transforming Chromophoric Silver Clusters in DNA Nanoreactors. *Anal. Chem.* **2012**, *84*, 356–364.
- (51) Petty, J. T.; Ganguly, M.; Rankine, I. J.; Baucum, E. J.; Gillan, M. J.; Eddy, L. E.; Léon, J. C.; Müller, J. Repeated and Folded DNA Sequences and Their Modular Ag106+ Cluster. *J. Phys. Chem. C* 2018, 122, 4670–4680.
- (52) Petty, J. T.; Ganguly, M.; Rankine, I. J.; Chevrier, D. M.; Zhang, P. A DNA-Encapsulated and Fluorescent Ag_{10}^{6+} Cluster with a Distinct Metal-Like Core. *J. Phys. Chem. C* **2017**, *121*, 14936–14945.
- (53) Petty, J. T.; Sergev, O. O.; Ganguly, M.; Rankine, I. J.; Chevrier, D. M.; Zhang, P. A Segregated, Partially Oxidized, and Compact Ag₁₀ Cluster within an Encapsulating DNA Host. *J. Am. Chem. Soc.* **2016**, 138, 3469–3477.
- (54) Banerjee, S.; Mazumdar, S. Electrospray Ionization Mass Spectrometry: A Technique to Access the Information Beyond the Molecular Weight of the Analyte. *Int. J. Anal. Chem.* **2012**, 2012, 282574.
- (55) Dertinger, T.; Pacheco, V.; von der Hocht, I.; Hartmann, R.; Gregor, I.; Enderlein, J. Two-Focus Fluorescence Correlation Spectroscopy: A New Tool for Accurate and Absolute Diffusion Measurements. *ChemPhysChem* **2007**, *8*, 433–443.
- (56) Gendron, P. O.; Avaltroni, F.; Wilkinson, K. J. Diffusion Coefficients of Several Rhodamine Derivatives as Determined by

- Pulsed Field Gradient-Nuclear Magnetic Resonance and Fluorescence Correlation Spectroscopy. *J. Fluoresc.* **2008**, *18*, 1093–101.
- (57) Petty, J. T.; Sergev, O. O.; Nicholson, D. A.; Goodwin, P. M.; Giri, B.; McMullan, D. R. A Silver Cluster—DNA Equilibrium. *Anal. Chem.* **2013**, *85*, 9868—9876.
- (58) Obliosca, J. M.; Babin, M. C.; Liu, C.; Liu, Y. L.; Chen, Y. A.; Batson, R. A.; Ganguly, M.; Petty, J. T.; Yeh, H. C. A Complementary Palette of Nanocluster Beacons. *ACS Nano* **2014**, *8*, 10150–60.
- (59) Akers, G. K. Molecular Sieve Methods of Analysis. In *The Proteins*; Neurath, H., Hill, R. L., Eds.; Academic Press: New York, 1975; Vol. 1, p 547.
- (60) Doose, S.; Barsch, H.; Sauer, M. Polymer Properties of Polythymine as Revealed by Translational Diffusion. *Biophys. J.* **2007**, 93, 1224–1234.
- (61) Tuma, R. S.; Beaudet, M. P.; Jin, X.; Jones, L. J.; Cheung, C.-Y.; Yue, S.; Singer, V. L. Characterization of Sybr Gold Nucleic Acid Gel Stain: A Dye Optimized for Use with 300-Nm Ultraviolet Transilluminators. *Anal. Biochem.* 1999, 268, 278–288.
- (62) Sanborn, M. E.; Connolly, B. K.; Gurunathan, K.; Levitus, M. Fluorescence Properties and Photophysics of the Sulfoindocyanine Cy3 Linked Covalently to DNA. *J. Phys. Chem. B* **2007**, *111*, 11064–11074.
- (63) Koszinowski, K.; Ballweg, K. A Highly Charged Ag₆⁴⁺ Core in a DNA-Encapsulated Silver Nanocluster. *Chem. Eur. J.* **2010**, *16*, 3285–3290.
- (64) Yamane, T.; Davidson, N. On the Complexing of Deoxyribonucleic Acid by Silver(I). *Biochim. Biophys. Acta* **1962**, *55*, 609–621.
- (65) O'Neill, P. R.; Velazquez, L. R.; Dunn, D. G.; Gwinn, E. G.; Fygenson, D. K. Hairpins with Poly-C Loops Stabilize Four Types of Fluorescent Agn:DNA. *J. Phys. Chem. C* **2009**, *113*, 4229–4233.
- (66) Dolamic, I.; Knoppe, S.; Dass, A.; Bürgi, T. First Enantioseparation and Circular Dichroism Spectra of Au₃₈ Clusters Protected by Achiral Ligands. *Nat. Commun.* **2012**, *3*, 798.
- (67) Hooley, E. N.; Paolucci, V.; Liao, Z.; Carro Temboury, M. R.; Vosch, T. Single-Molecule Characterization of near-Infrared-Emitting Silver Nanoclusters. *Adv. Opt. Mater.* **2015**, *3*, 1109–1115.
- (68) Petty, J. T.; Fan, C.; Story, S. P.; Sengupta, B.; St. John Iyer, A.; Prudowsky, Z.; Dickson, R. M. DNA Encapsulation of 10 Silver Atoms Producing a Bright, Modulatable, near-Infrared-Emitting Cluster. *J. Phys. Chem. Lett.* **2010**, *1*, 2524–2529.
- (69) Xu, W. W.; Zeng, X. C.; Gao, Y. The Structural Isomerism in Gold Nanoclusters. *Nanoscale* **2018**, *10*, 9476–9483.
- (70) Copp, S. M.; Schultz, D.; Swasey, S. M.; Faris, A.; Gwinn, E. G. Cluster Plasmonics: Dielectric and Shape Effects on DNA-Stabilized Silver Clusters. *Nano Lett.* **2016**, *16*, 3594–3599.
- (71) Swasey, S. M.; Karimova, N.; Aikens, C. M.; Schultz, D. E.; Simon, A. J.; Gwinn, E. G. Chiral Electronic Transitions in Fluorescent Silver Clusters Stabilized by DNA. *ACS Nano* **2014**, *8*, 6883–92
- (72) Pils, W.; Micura, R. Flexible Non-Nucleotide Linkers as Loop Replacements in Short Double Helical Rnas. *Nucleic Acids Res.* **2000**, 28, 1859–1863.
- (73) Tarasow, T. M.; Tinnermeier, D.; Zyzniewski, C. Characterization of Oligodeoxyribonucleotide—Polyethylene Glycol Conjugates by Electrospray Mass Spectrometry. *Bioconjugate Chem.* **1997**, *8*, 89–93.
- (74) Ono, A.; Cao, S.; Togashi, H.; Tashiro, M.; Fujimoto, T.; MacHinami, T.; Oda, S.; Miyake, Y.; Okamoto, I.; Tanaka, Y. Specific Interactions between Silver(I) Ions and Cytosine-Cytosine Pairs in DNA Duplexes. *Chem. Commun.* **2008**, 4825–4827.
- (75) Mandal, S.; Müller, J. Metal-Mediated DNA Assembly with Ligand-Based Nucleosides. *Curr. Opin. Chem. Biol.* **2017**, *37*, 71–79. (76) Baik, M.-H.; Silverman, J. S.; Yang, I. V.; Ropp, P. A.; Szalai, V. A.; Yang, W.; Thorp, H. H. Using Density Functional Theory to Design DNA Base Analogues with Low Oxidation Potentials. *J. Phys. Chem. B* **2001**, *105*, 6437–6444.

- (77) Wagenknecht, H.-A. Electron Transfer Processes in DNA: Mechanisms, Biological Relevance and Applications in DNA Analytics. *Nat. Prod. Rep.* **2006**, 23, 973–1006.
- (78) O'Neill, P. R.; Gwinn, E. G.; Fygenson, D. K. UV Excitation of DNA Stabilized Ag Cluster Fluorescence via the DNA Bases. *J. Phys. Chem. C* **2011**, *115*, 24061–24066.
- (79) Brouwer, A. M. Standards for Photoluminescence Quantum Yield Measurements in Solution. *Pure Appl. Chem.* **2011**, 83, 2213–2228.

A DNA-Encapsulated Silver Cluster and the Roles of Its Nucleobase Ligands

Jeffrey T. Petty, *+^ Mainak Ganguly, +^ Ahmed I. Yunus, + Chen He, + Peter M. Goodwin, # Yi-Han Lu, o and Robert M. Dickson o

⁺Department of Chemistry, Furman University, Greenville, SC 29163

[#] Center for Integrated Nanotechnologies, Mail Stop K771, Los Alamos National Laboratory, Los Alamos, New Mexico 87545

^o School of Chemistry and Biochemistry and Institute for Bioengineering & Bioscience, Georgia Institute of Technology, Atlanta, Georgia 30332

Corresponding author's email address: jeff.petty@furman.edu

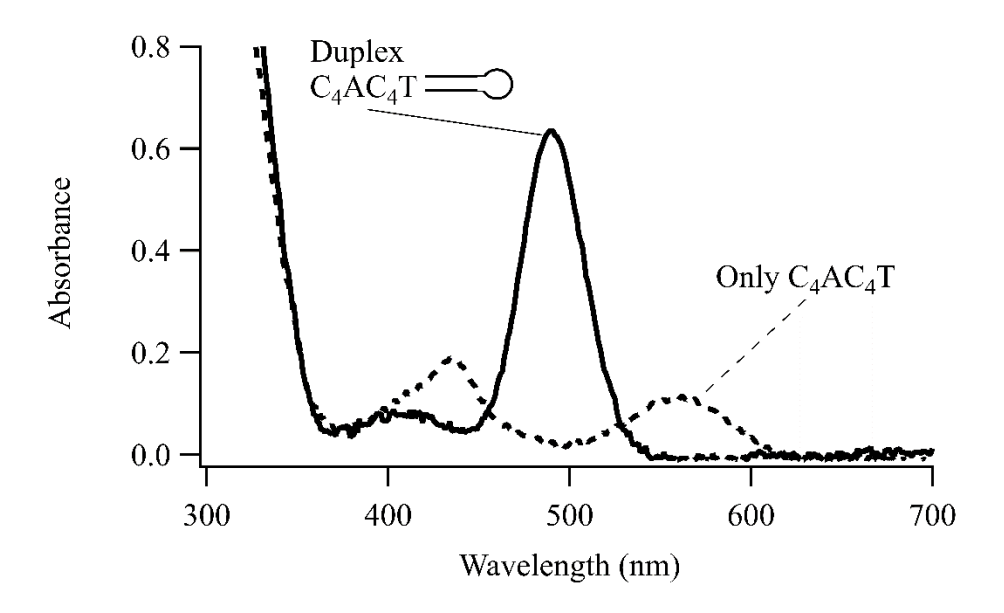


Figure S1: Absorption spectra of C₄AC₄T duplex (solid) and C₄AC₄T alone (dashed). Without the duplex appendage, the target $\lambda = 490$ nm cluster does not form. The duplex is the hairpin CCCG TT CGGG that has a melting temperature ~37 °C. ¹

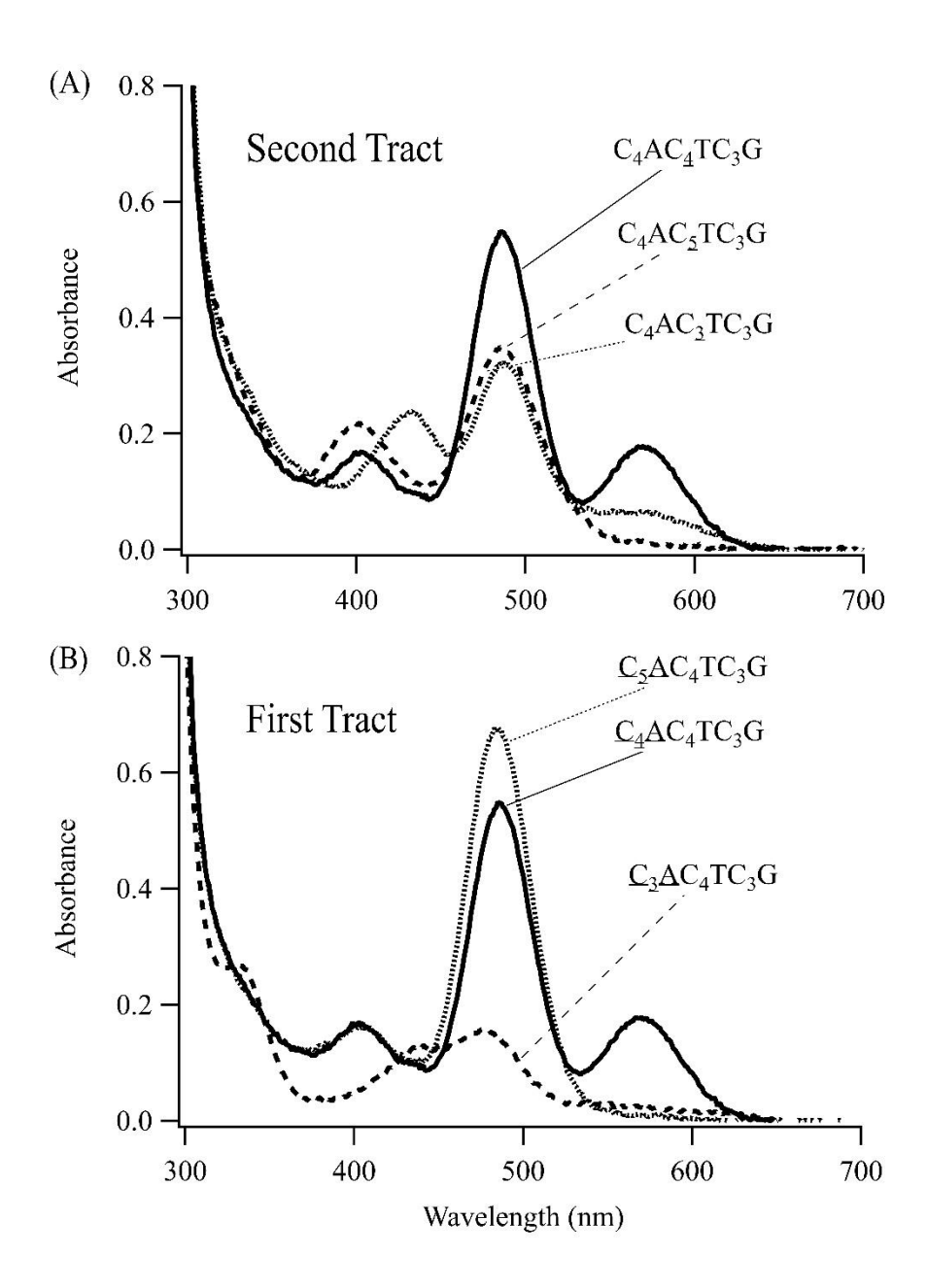


Figure S2: Absorption spectra show that the number of cytosines controls the cluster environment. (A) The second tract with C_4T gives the strongest A_{490} relative to C_5T and C_4T . (B) The first tract with C_4A and C_5A gives stronger A_{490} relative to C_3A .

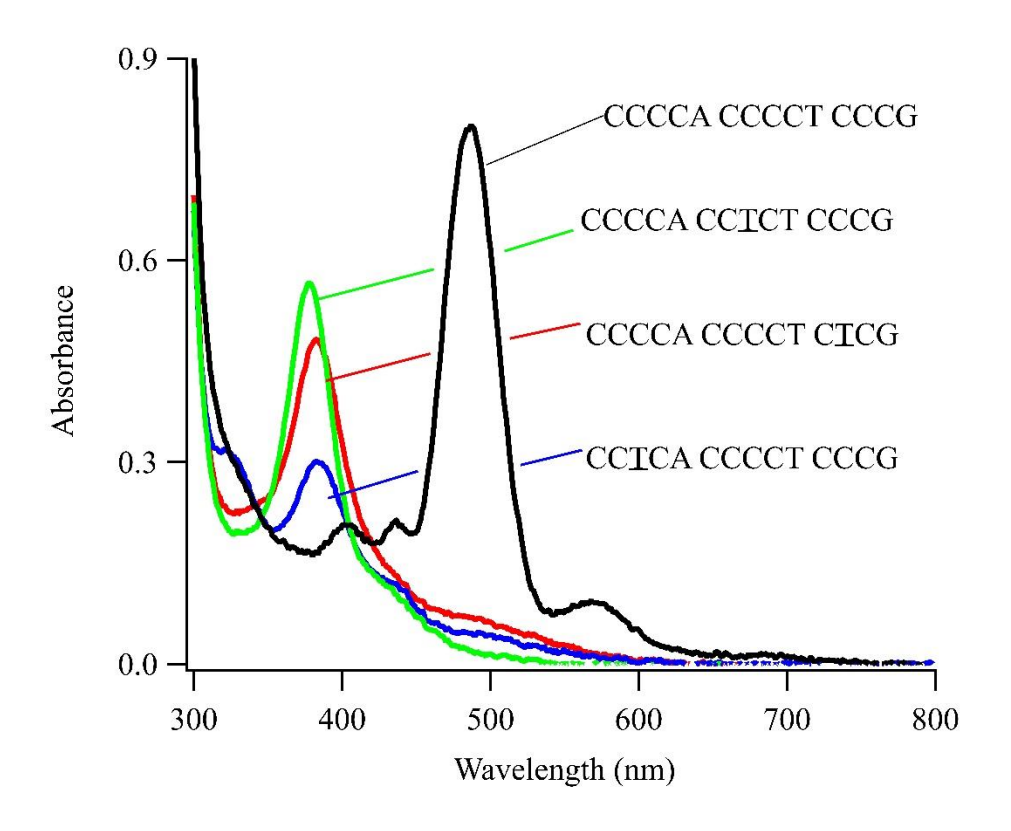


Figure S3: The oligonucleotide $C_4AC_4TC_3G$ (black) yields strong absorption at 490 nm. This sequence was modified by substituting a cytosine with a thymine, which is a weaker ligand for silver at neutral pH. Single cytosines in the first (blue), second (green), and third (red) tracts were replaced with a thymine, and each modified strand yielded the same result, i.e. they eliminated the 490 nm absorption in favor of transitions at \sim 380 nm.

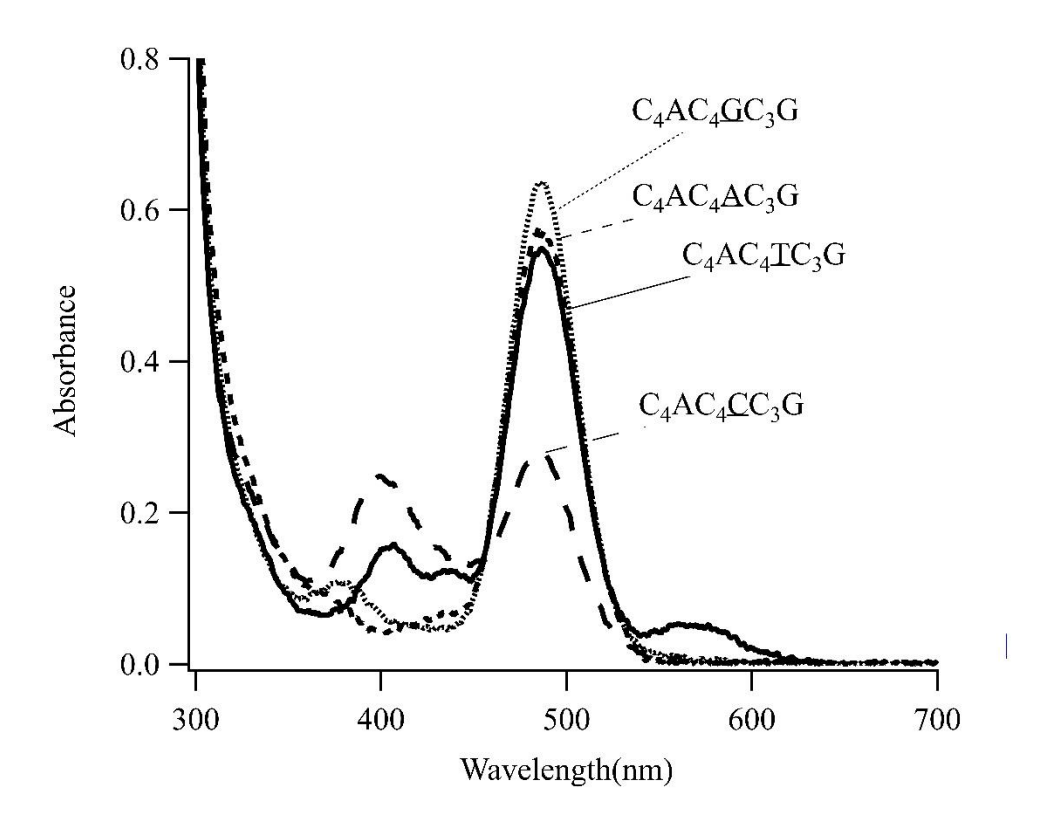


Figure S4: Absorption spectra of $C_4AC_4YC_3G$ sequences with Y = G (dotted), A (dashed), T (solid), and C (long dashed). The former three sequences yield similar spectra whereas the latter sequence also favors a violet species and is less selective for the 490 nm cluster.

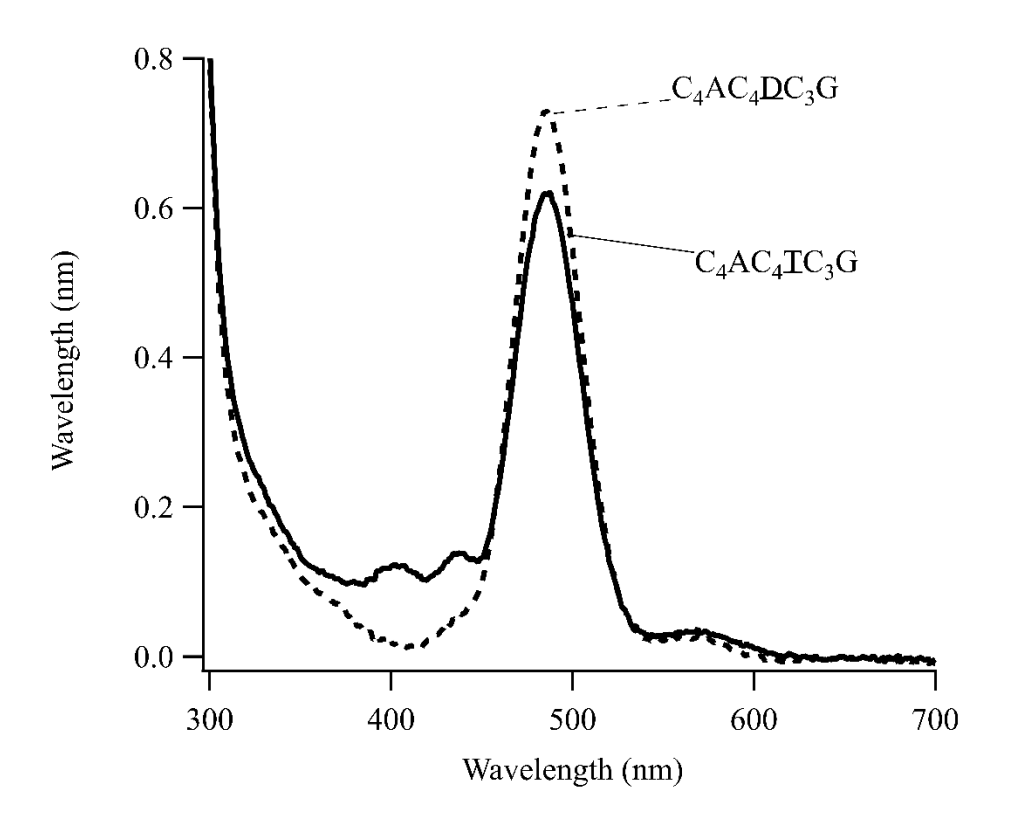


Figure S5: Absorption spectra of $C_4AC_4YC_3G$ with Y = D/abasic site (dashed) and T (solid line) that yield the same 490 nm cluster with similar absorbances.

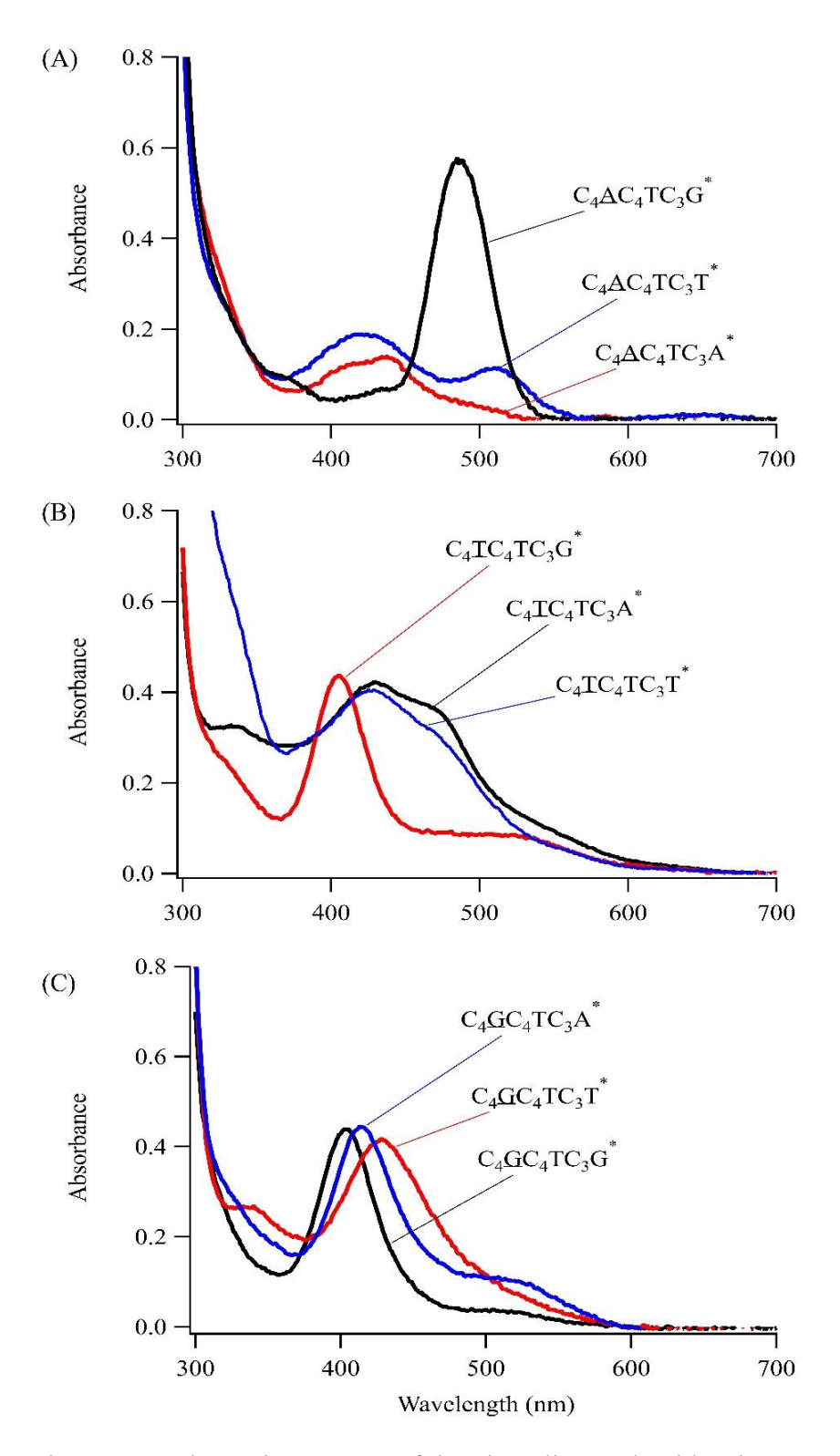


Figure S6: Absorption spectra of the nine oligonucleotides that vary the terminal nucleobases in the first and third tracts while maintaining thymine in the second tract. The underlined nucleobases were fixed to be adenine (A), thymine (B), and guanine (C) in the first tract. The starred nucleobases in the third tract were varied.

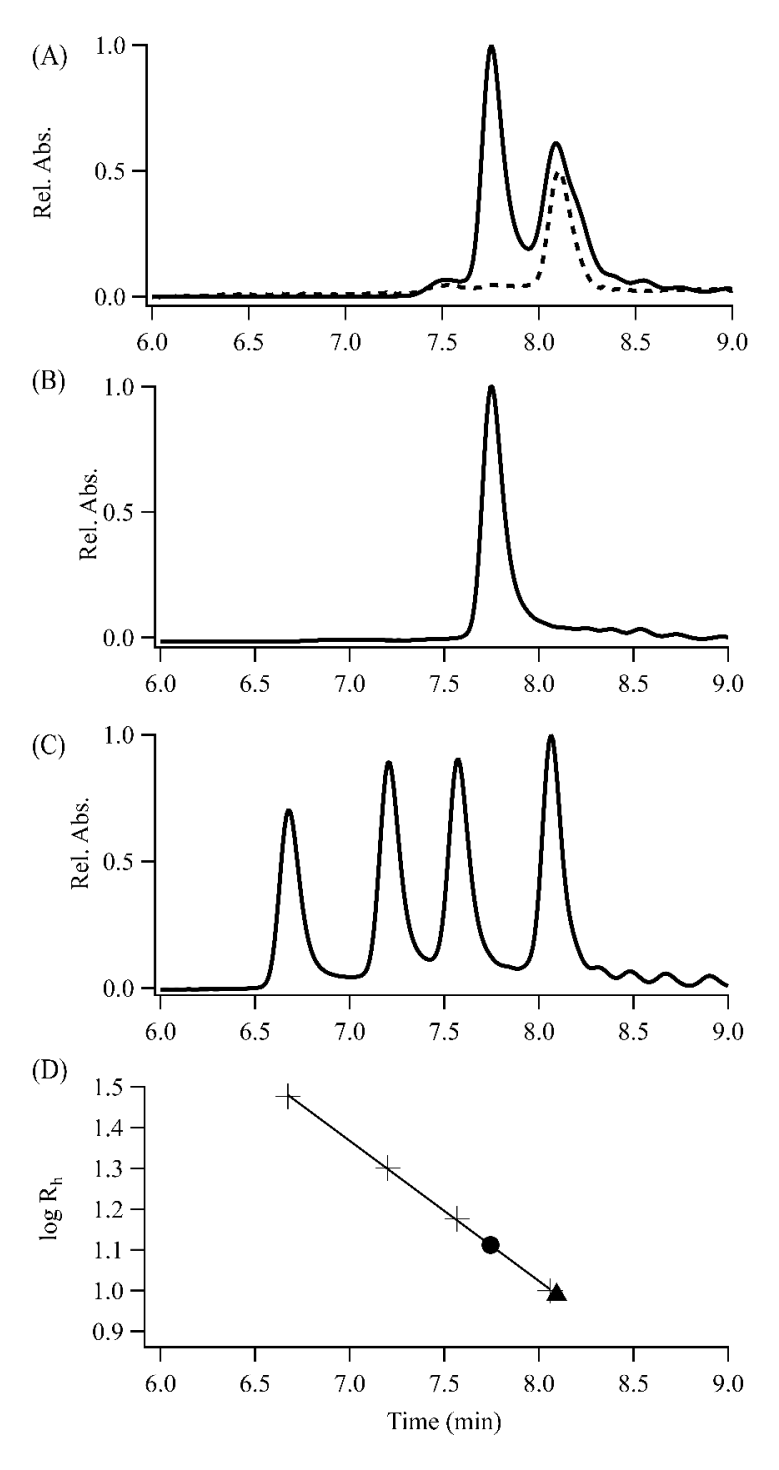


Figure S7: Size exclusion chromatograms of the cluster-DNA complex (A) with absorption measured at 260 (solid) and 490 nm (dotted), of the DNA alone (B), and of the mixture of dT_{10} , dT_{15} , dT_{20} , and dT_{30} (C). The calibration plot (D) is based on the retention times and hydrodynamic radii of the thymine strands (crosses). The retention time of the oligonucleotide is indicated by a circle and elutes as a dT_{13} . The DNA-cluster complex elutes as a dT_{10} and is thus more compact.

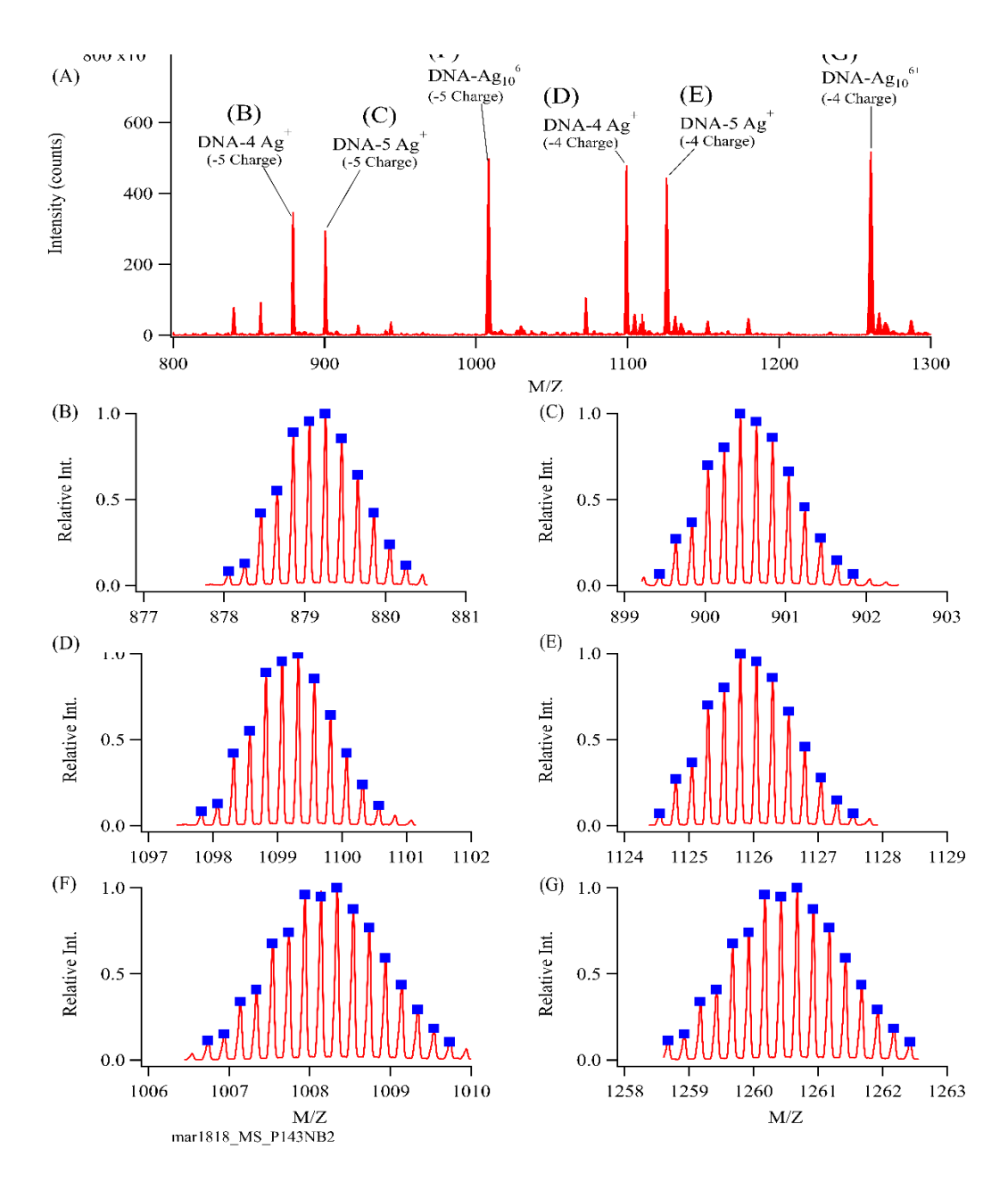


Figure S8. (A) Mass:charge spectrum of a $C_4AC_4(TEG)C_3G$ complexes with 4, 5, and 10 silvers. (B)-(F) Expanded view of the -4 and -5 charge states for these ions. The blue tick marks represent the predicted masses based on the following molecular formulas: $C_{125}H_{161}O_{81}N_{43}P_{13}Ag_4^{-5}$ (B), $C_{125}H_{160}O_{81}N_{43}P_{13}Ag_5^{-5}$ (C), $C_{125}H_{162}O_{81}N_{43}P_{13}Ag_4^{-4}$ (D), $C_{125}H_{161}O_{81}N_{43}P_{13}Ag_5^{-4}$ (E), $C_{125}H_{159}O_{81}N_{43}P_{13}Ag_{10}^{-5}$ (F), and $C_{125}H_{160}O_{81}N_{43}P_{13}Ag_{10}^{-4}$ (G). Note that the fully protonated strand has the molecular formula $C_{125}H_{170}O_{81}N_{43}P_{13}$. The precisions between the observed and predicted masses of the isotopologues are 2.2 ± 0.2 (B), 1.9 ± 0.4 (C), 2.4 ± 0.2 (D), 2.4 ± 0.6 (E), 1.7 ± 0.2 (F), and 1.7 ± 0.2 ppm.

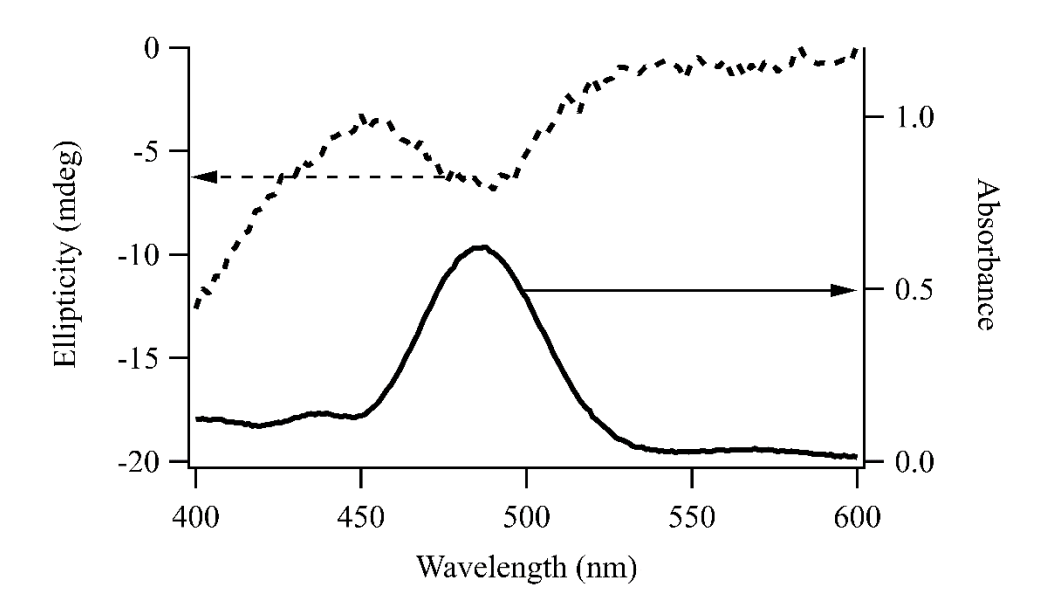


Figure S9: Circular dichroism spectra (dotted) and absorption (solid) spectra of the silver cluster with the $C_4AC_4TC_3G$ strand.

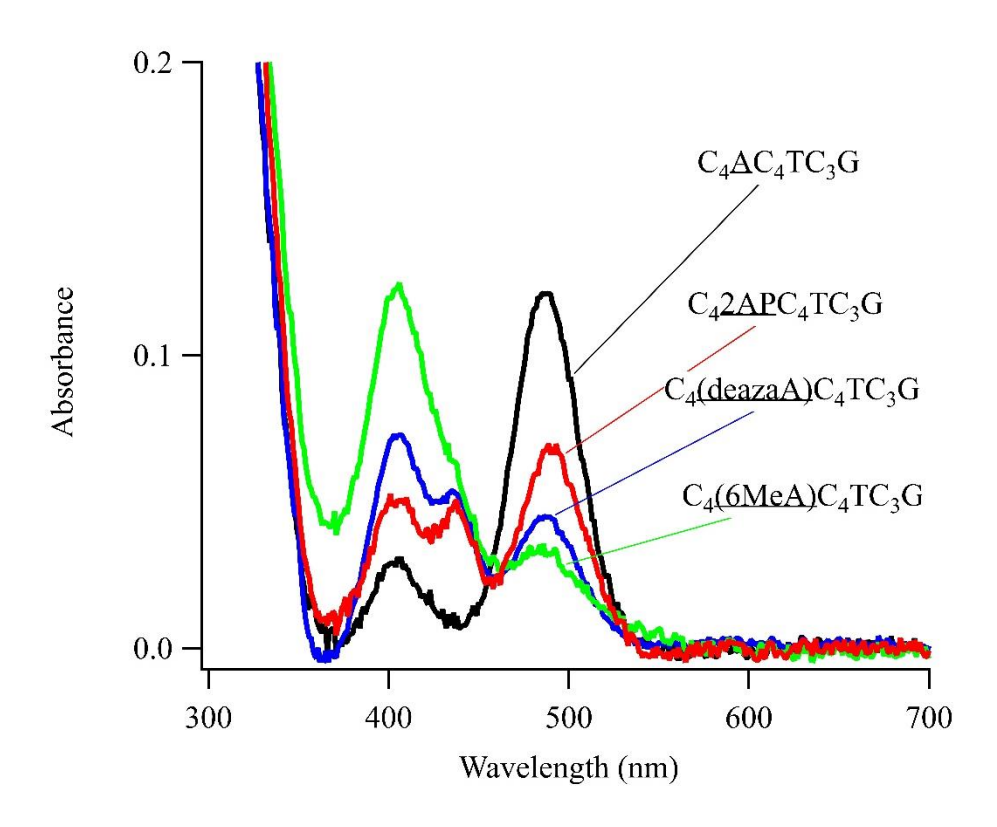


Figure S10: Absorption spectra for $C_4XC_4TC_3G$ derivatives with X = 6-methylyadenine (green), 7-deazaadenine (blue), 2-aminopurine (red), and adenine (black).

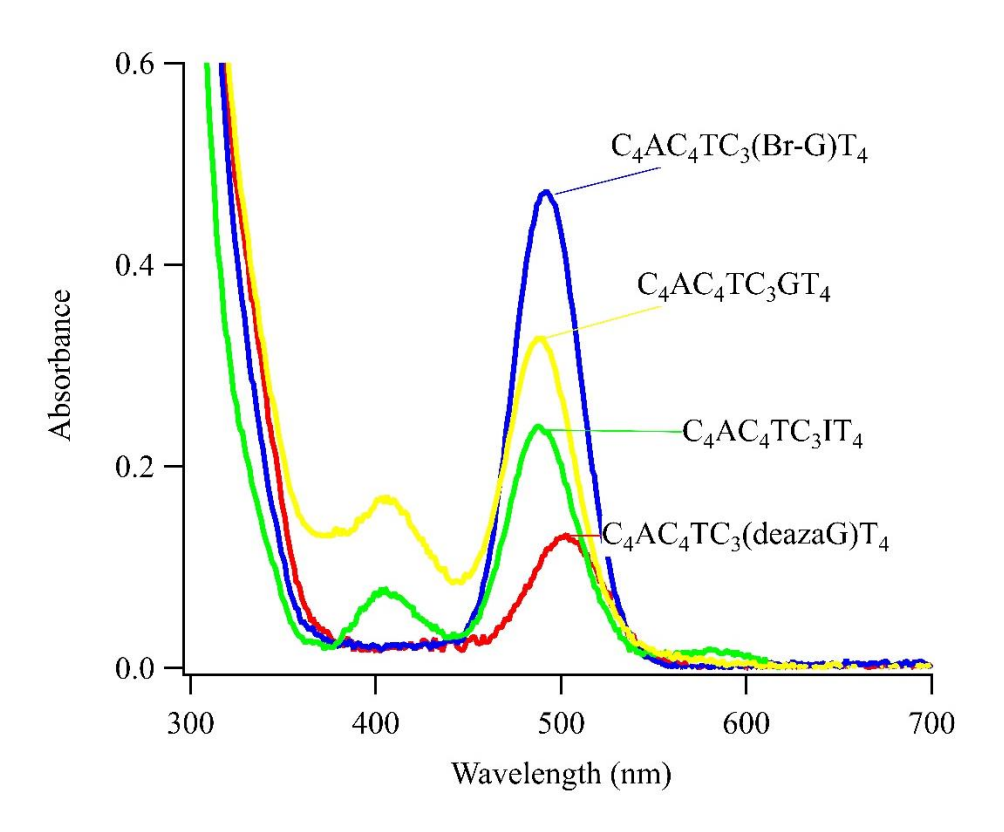


Figure S11: Absorption spectra for the $C_4AC_4TC_3ZT_4$ derivatives with Z = 7-deazaguaine (red), inosine (green), guanine (yellow), and 8-bromoguanine (blue).

¹ Zadeh, J. N.; Steenberg, C. D.; Bois, J. S.; Wolfe, B. R.; Pierce, M. B.; Khan, A. R.; Dirks, R. M.; Pierce, N. A. Nupack: Analysis and Design of Nucleic Acid Systems. *Journal of Computational Chemistry* **2011**, *32*, 170-173.